Coupled thermo-hydro-mechanical modelling of carbon dioxide sequestration in saline aquifers considering phase change

Weiyong Lu[1,*] and Xin Zhang[2]

[1]School of Mines, Luliang University, Lvliang, Shanxi 033000, China
[2]School of Minerals and Energy Resources Engineering, Faculty of Engineering, University of New South Wales, Sydney NSW 2052, Australia

Carbon dioxide (CO_2) sequestration in saline aquifers is considered to be one of the most viable measures to control its emissions. During the process of CO_2 injection, phase changes of gas, liquid and supercritical CO_2 will lead to changes in the density, dynamic viscosity, specific heat capacity and CO_2 heat conductivity and solubility in water, which will influence the injection pressure and spatial distribution of CO_2. To study the characteristics of injection pressure and spatial distribution of CO_2 in saline aquifers, equations of state such as Peng–Robinson equation were used to realize the continuous calculation of the physical property parameters of gas, liquid and supercritical CO_2. Based on the continuous physical property parameters, a fully thermo-hydro-mechanical (THM) coupled model was developed and then solved and verified using COMSOL Multiphysics software. It has been shown in this study that: (i) the predicted CO_2 injection pressure by the THM coupled model is higher than that obtained from the uncoupled model; (ii) at the top boundary of the reservoir, the spatial distribution of CO_2 can be divided into a rapid increase region, a slow decrease region, a rapid decrease region and an initial saturation region along the direction of CO_2 migration and (iii) larger the reservoir geothermal gradient, more obvious is the gravity override effect.

Keywords: Carbon dioxide sequestration, phase change, saline acquifers, thermo-hydro-mechanical modelling.

CARBON DIOXIDE (CO_2) is considered to be one of the main greenhouse gases (GHGs) that results in global warming of the earth's atmosphere[1,2]. Methods to effectively dispose of man-made CO_2 is important now. CO_2 capture and storage (CCS) is one of the most effective methods to reduce massive CO_2 emissions into the atmosphere[3,4]. At present, deep saline aquifers, depleted oil, gas and coal reservoirs and salt caverns are considered to be the major geological sequestration media for the next 10–100 years. Deep saline aquifers with large storage capacity and global scope are widely distributed. It is estimated that nearly 600 billion tonnes of CO_2, which is equivalent to the total man-made CO_2 production in the next 20 years, can be stored in saline aquifers of the Utsira sandstone reservoirs of the Sleipner field in Norway[5,6].

At present, 15 large commercial CCS projects are being conducted in the Salah of Algeria, the Snøhvit and Sleipner gas fields of Norway, and the Quest project in Canada[7]. According to the research statistics, seven billion tonnes of CO_2 worldwide, needs to be disposed of yearly by geologic sequestration to effectively control man-made CO_2 emissions[5]. A series of physical and chemical changes will occur with massive CO_2 injection into saline aquifers, including multiphase fluid flow, change in effective stresses in the saline aquifers, dissolution of CO_2 in brine and chemical reactions in brine, reservoir rock minerals and CO_2.

CO_2 sequestration in deep saline aquifers is a complex, mutually coupled process of seepage fields, stress fields and temperature fields. To describe this complex process, a series of mathematical models have been developed and are gradually being modified. The developed and modification of models has led to the development process from considering a single seepage field to hydro-mechanical coupled fields and then to thermo-hydro-mechanical (THM) coupled fields[3,7–12]. Numerical simulation is considered as the most suitable method to study the complex relation among different fields during CO_2 sequestration. By solving the coupled equations of numerical simulation, the mechanism of CO_2 sequestration can be better understood. Moreover, CO_2 storage locations can be properly selected by accurate calculation of storage capacity, and the CO_2 injection pressure and its spatial distribution in the aquifers can be effectively predicted. CO_2 injection pressures can also be controlled to prevent cap rock fracture, which would lead to sequestrated CO_2 leaking into the atmosphere[13–17].

The THM coupled model used in this study consists of the mechanical equilibrium equation, mass continuity equation and equation of energy conservation. The physical parameters of CO_2 density, dynamic viscosity, specific

*For correspondence. (e-mail: 489698551@qq.com)

heat capacity, thermal conductivity coefficient and solubility of CO_2 in water are used in these three equations. The physical parameters of CO_2 will change with changes in environmental temperature and pressure.

Under standard conditions, CO_2 can be considered an ideal gas with a density of 1.872 kg/m^3. The pressure and temperature in saline aquifers are usually higher than the critical temperature (304.25 K) and critical pressure (7.39 MPa) of CO_2. Under such conditions, the density of CO_2 is similar to that of a liquid, whereas its dynamic viscosity is close to that of a gas. This CO_2 state is called the supercritical state. During injection of CO_2 from the ground into deep saline aquifers, the CO_2 phase will change from gas to liquid and then to the supercritical state. Therefore, it is impractical to consider CO_2 density as a constant. Moreover, the ideal equation of state (EoS) of a gas can be used to calculate the density of CO_2 in the gaseous state. To calculate density of CO_2 in its different states (gas, liquid and supercritical according to one formula), the Peng–Robinson state equation, and the Span and Wagner state equation have been developed[7,18].

Although coupled models of the geologic sequestration process have been continuously improved, currently some disadvantages remain in the models used. Using the Peng–Robinson state equation, and the Span and Wagner state equation, the fully coupled model can be used to calculate the density of CO_2 in different states. However, other physical parameters, such as dynamic viscosity, specific heat capacity, thermal conductivity coefficient and solubility of CO_2 in water cannot be calculated.

To study the effects of changing physical parameters on the CO_2 injection process, we first studied the calculation models for CO_2 density, dynamic viscosity, specific heat capacity, thermal conductivity coefficient and CO_2 solubility in brine. The physical parameters of CO_2 in different states were then calculated using the calculation models. Then, we established a THM coupled model for CO_2 in gas, liquid and supercritical states. Based on the THM coupled model, the injection pressure and spatial distribution of CO_2 under the coupled THM effect were then determined.

Thermodynamic properties of CO_2

Calculation model for density of CO_2

At present, cubic EoSs is mainly used to determine the phase state of fluids, among which the Peng–Kwong (PK) EoS, Soave–Redlich–Kwong (SRK) EoS, Peng–Robinson EoS, and experience Redlich–Kwong (EXP-RK) EoS are relatively typical. Comparative analysis shows that the Peng–Robinson EoS has the highest accuracy for calculating density of CO_2 under different temperatures and pressure[18,19]. The Peng–Robinson EoS is expressed as follows[20]

$$P = \frac{RT}{V-b} - \frac{a(T)}{V(V+b)+b(V-b)}, \tag{1}$$

where

$$\begin{cases} a(T) = 0.457235R^2T_{\text{cri}}^2\alpha(T)/P_{\text{cri}}, \\ \alpha(T) = [1+0.37646+1.5426\omega-0.26992\omega^2)(1-\sqrt{T_t})]^2, \\ b = 0.077796RT_{\text{cri}}/P_{\text{cri}}, \\ T_{\text{r}} = T/T_{\text{cri}}. \end{cases} \tag{2}$$

Here R is the universal gas constant (8.314 J/(mol K)), a and b are parameters of the EoS, P_{cri} the critical pressure of the CO_2 phase, T_{cri} the critical temperature of the CO_2 phase, w the eccentric factor (0.239) and T_{r} is the reduced temperature.

By substituting the CO_2 density $\rho_{\text{c}} = m/V$ into eq. (1) it can be simplified as follows

$$(b^3P + b^2RT - ab)\rho_{\text{c}}^3 - (3b^2P + 2bRT - a)M_{\text{c}}\rho_{\text{c}}^2 + (Pb - RT)M_{\text{c}}^2\rho_{\text{c}} + PM_c^3 = 0, \tag{3}$$

where ρ_{c} is the CO_2 density and M_{c} is the molar mass of CO_2.

Equation (3) is a simple cubic equation of ρ_{c} with three roots by which the phase state of CO_2 can be determined[21]. If the roots of eq. (3) consist of a real number and two imaginary numbers, the phase of CO_2 is gas or liquid, determined by the temperature and pressure. If the roots of eq. (3) are three different real numbers, two phases of gas and liquid of CO_2 exist at the same time. The maximum root is the density of liquid CO_2, the minimum root is the density of gaseous CO_2, and the middle root has no physical significance. If the three roots are equal, the CO_2 fluid is in a supercritical phase, and the root value is the density of the supercritical CO_2. Figure 1 *a* shows the density of CO_2 in gaseous, liquid and supercritical states calculated by the Peng–Robinson EoS. The figure illustrates that the density of CO_2 is highly sensitive to changes of temperature and pressure. Near the critical point, the density of CO_2 changes drastically with change in temperature and pressure because the phase of CO_2 changes near the critical point.

Calculation model for dynamic viscosity of CO_2

The dynamic viscosity of CO_2 is a function of temperature and pressure. The phases of CO_2 are different under different temperatures and pressures, and the dynamic viscosities of gaseous and liquid CO_2 are usually calculated using different models. In the continuous transition of CO_2 from gas to liquid, conventional methods of

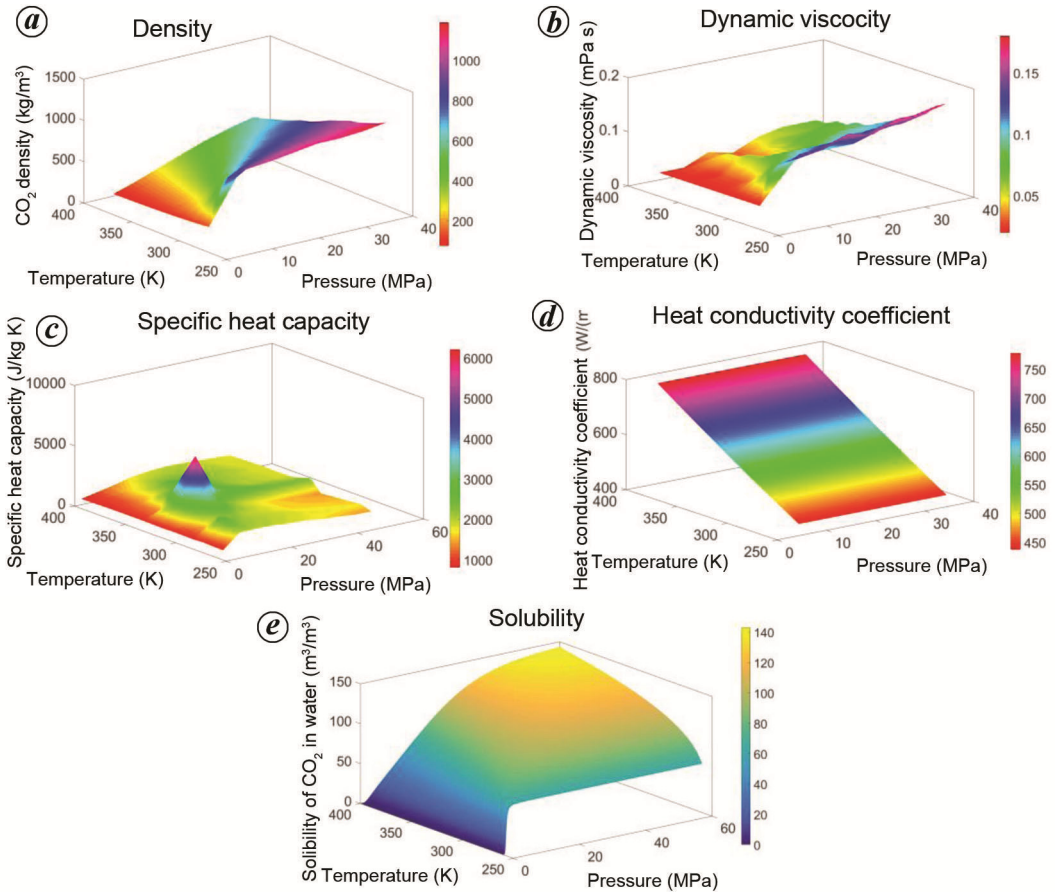

Figure 1 ***a–e.*** Relationship between thermodynamic parameters of carbon dioxide (CO_2) and pressure and temperature.

calculation are no longer applicable for the dynamic viscosity of CO_2. Based on the Peng–Robinson EoS, a new calculation model for dynamic viscosity was established[25] which can be used to calculate the dynamic viscosity of CO_2 in the gas, liquid and supercritical phases. The formula for CO_2 dynamic viscosity can be expressed as follows[22–24]

$$T\mu_c^3 + (2bT - b'T - r'P)\mu_c^2 -$$

$$(2bb'T + Tb^2 + 2r'bP - a)\mu_c + (Tb'b^2 + r'Pb^2 - ab') = 0, \quad (4)$$

where

$$a = 0.45724 r_c^2 P_c^2 / T_c^2,\ b = 0.07780 r_c^2 P_c^2 / T_c^2,$$

$$\mu_c = 7.7 T_c^{-1/6} M^{0.5} P_c^{2/3},$$

$$r' = r\tau(T_r, P_r),\ b' = b\phi\tau(T_r, P_r),\ \tau(T_r, P_r)$$

$$= [1 + Q_1(\sqrt{P_r T_r} - 1)]^{-2},$$

$$P_r = P/P_c,\ T_r = T/T_c,$$

$$Q_1 = 0.829599 + 0.350867w - 0.747680w^2,$$

μ_c is the dynamic viscosity of CO_2, and ϕ is the pore ratio.

Figure 1 *b* shows the results of applying eq. (4) to calculate the dynamic viscosity of CO_2 fluid under different temperatures and pressures.

Calculation model for specific heat capacity of CO_2

The calculation models for CO_2 specific heat capacity can be classified into two categories: models for gaseous CO_2 and those for liquid CO_2. The Sterling–Brown equation is generally used to calculate the specific heat capacity of liquid CO_2. Because of the phase change of CO_2, a calculation model for the specific heat capacity of CO_2 in different phases should be selected. We used the calculation model for specific heat capacity of CO_2 based on the Peng–Robinson EoS; it can be used to calculate the specific heat capacity of CO_2 in any phase and is expressed as follows[25,26]

$$C_{pc} = C_p^* + DC_p = C_p^* + (Z - 1)R$$

$$+ \frac{0.6766P}{ZRT^2 + 29.7903 \times 10^{-6} PT}, \quad (5)$$

where C_{pc} is the specific heat capacity of the fluid at constant pressure, ΔC_p the deviation of specific heat capacity

at constant pressure, Z the compressibility factor ($Z = PV/RT$), T the temperature and C_p^* is the specific heat capacity of an ideal gas under constant pressure, given by $C_p^* = A + BT + CT^2 + DT^3$, where $A = 4.728$, $B = 1.754 \times 10^{-2}$, $C = -2.338 \times 10^{-5}$, and $D = 4.079 \times 10^{-9}$.

In general, the injection pressure of CO_2 is 5–35 MPa, and the injection temperature is 253–393 K. Figure 1 *c* shows the calculated specific heat capacities of CO_2 under different pressures and temperatures using eq. (5). The figure illustrates that a peak point of the specific heat capacity of CO_2 occurs near the critical region. This indicates that the phase change of CO_2 has a great effect on its specific heat capacity.

Calculation model for heat conductivity coefficient of CO_2

The heat conductivity coefficient of CO_2 is a function of temperature and pressure. Under different temperatures and pressures, the heat conductivity coefficient changes with the CO_2 phase. We used the calculation model for heat conductivity of CO_2 as follows[23,27]

$$(\lambda_c - \lambda_{c0})\Gamma Z_c^5 = \begin{cases} 1.22 \times 10^{-2}(e^{0.535\rho_r} - 1), & \rho_r < 0.5, \\ 1.14 \times 10^{-2}(e^{0.67\rho_r} - 1.069), & 0.5 \le \rho_r \le 2.0, \\ 2.60 \times 10^{-3}(e^{1.155\rho_r} + 2.016), & 2.0 < \rho_r < 2.8, \end{cases} \quad (6)$$

where λ_{c0} is the heat conductivity of supercritical CO_2 at atmospheric pressure

$$\lambda_{c0} = 10^{(1.307\log_{10}T - 0.5)} \text{ and } \Gamma = 1.431 \times 10^7 (T_{cri}M^3/\rho_{cri}^4)^{1/6}.$$

Figure 1 *d* shows the calculation model for heat conductivity coefficient of CO_2. The figure indicates that temperature and pressure have significant effects on the heat conductivity of CO_2. The heat conductivity coefficient of CO_2 in the energy conservation equation should be modified by the calculation model of eqs (6) to (7) account for changes in temperature and pressure in the reservoir during the migration of CO_2 in saline aquifers.

Solubility of CO_2 in saline water

The solubility of CO_2 in brine is non-negligible with an increase in temperature and pressure[28]. We used the calculation model for solubility of CO_2 in brine as follows[29]

$$\rho_{dc} = \frac{0.178094}{\left[\begin{array}{c} A_1\rho_w^{A_2}(1.8T - 459.67)^{A_7} + A_3(1.8T - 459.67)^{A_4} \\ \times \exp[-145.0377A_5p + A_6/(145.0377p)] \end{array}\right]}, \quad (7)$$

where ρ_{dc} is the CO_2 solubility in brine and A_1, A_2, A_3, A_4, A_5, A_6 and A_7 are the parameters of the calculation model, whose values are 0.004934, 4.0928, 5.71×10^{-7}, 1.6428, 6.763×10^{-4}, 781.334 and –0.2499 respectively.

The THM coupled modelling framework

Mass conservation equation

During the flow of water and CO_2 in saline aquifers, the dissolution of water and CO_2 in each other will occur. If the dissolution of water in CO_2 is ignored and only the dissolution of CO_2 in water is considered, the mass conservation equations for water and CO_2 can be written as follows

$$\begin{cases} \underbrace{\dfrac{\partial(\phi S_w\rho_w)}{\partial t} + \nabla(\rho_w\vec{v}_w) = 0}_{\text{Liquid water}} \\ \underbrace{\dfrac{\partial(\phi(1-S_w)\rho_c)}{\partial t} + \nabla(\rho_c\vec{v}_c)}_{\text{Supercritical/liquid/gas } CO_2} + \underbrace{\dfrac{\partial(\phi S_w\rho_{dc})}{\partial t} + \nabla(\rho_{dc}\vec{v}_c)}_{\text{Dissolved } CO_2 \text{ in water}} = 0, \end{cases} \quad (8)$$

where ϕ is the porosity of the saline aquifer, S_w the water saturation, ρ_w the density of water, ρ_w the velocity of water, t the time, ρ_c is the density of CO_2, which is determined by the reservoir temperature and pressure and can be calculated by eq. (3), v_c is the velocity of CO_2 and ρ_{dc} is the dissolution of CO_2 in water which is calculated by eq. (7).

The flow of water and CO_2 in porous media is governed by the generalized Darcy's law. The corresponding formula for fluid velocity is as follows

$$\boldsymbol{v}_{w,c} = -\frac{\boldsymbol{k}k_{rw,c}}{\mu_{w,c}}\nabla(p_{w,c} - \rho_{w,c}\boldsymbol{g}), \quad (9)$$

where $\boldsymbol{k}$ is the intrinsic permeability of rock, k_{rw} and k_{rc} the relative permeability of water and CO_2 respectively, μ_w the dynamic viscosity of water, μ_c the dynamic viscosity of CO_2, which can be calculated by eq. (4), and $\boldsymbol{g}$ is the acceleration due to gravity.

The density of water is influenced by pressure and temperature. The relationship of water density ρ_w with pressure and temperature can be expressed as follows

$$p_w = p_{w0}\exp[c_{wp}(p_w - p_{wref}) - c_{wT}(T_w - T_{wref})], \quad (10)$$

and

$$\begin{cases} c_{wp} = \dfrac{1}{\rho_w}\dfrac{\partial\rho_w}{\partial p_w} \\ c_{wT} = -\dfrac{1}{\rho_w}\dfrac{\partial\rho_w}{\partial T} \end{cases}, \quad (11)$$

where p_{wref} is the reference pressure whose value is 101.325 kPa under standard conditions, T_{wref} the reference temperature, whose value is 273 K under standard conditions and ρ_{w0} is the density of water under reference pressure and reference temperature.

Energy conservation equation

Heat exchange occurs within the system composed of water, CO_2 and saline aquifers by convection and heat transfer. To more accurately simulate the effect of the temperature field on CO_2 sequestration, the physical properties of CO_2, such as specific heat capacity and heat conductivity were considered in this study. Based on the law of energy conservation, the energy balance equation of the temperature field can be written as follows[30]

$$\frac{\partial}{\partial t}[(\rho C_p)_e T] + (\vec{v}_w \rho_w C_{pw} + \vec{v}_c \rho_c C_{pc})\nabla T$$
$$-\nabla \cdot (\lambda_e \nabla T) = Q_T, \tag{12}$$

and

$$\begin{cases} (\rho C_p)_e = \phi(S_w \rho_w C_{pw} + S_c p_c C_{pc}) + (1-\phi)\rho_s C_{ps} \\ \lambda_e = \phi[S_w \lambda_w + (1-S_w)\lambda_c] + (1-\phi)\lambda_s \\ Q_T = \phi Q_f + (1-\phi)Q_s \\ \vec{v}_{w,c} = -\dfrac{\boldsymbol{k} k_{rw,c}}{\mu_{w,c}}(\nabla p_{w,c} - \rho_{w,c}\boldsymbol{g}) \end{cases}, \tag{13}$$

where $(\rho C_p)_e$ is the effective heat capacity of the porous medium, C_{pw}, C_{pc} and C_{ps} are the specific heat capacity of water specie, CO_2 specie and porous media respectively, and C_{pc} can be calculated by eq. (5), λ_e is the effective heat conductivity coefficient, λ_w, λ_c and λ_s are the heat conductivity coefficient of water specie, CO_2 specie and porous media respectively, and λ_c can be calculated by eq. (6) and Q_f and Q_s are the heat source and heat sink of fluid and porous medium respectively, and $Q_f = Q_s = 0$ when the heat source and heat sink of rock are ignored.

Equation of mechanical balance

Reservoirs are usually porous media, the mechanical properties of which are influenced by pore characteristics, pore fluid pressure and reservoir temperature. Porous medium is generally considered to be a linearly elastic material. According to the generalized Hooke's law, the control equation of the stress field expressed by the displacement, pore fluid pressure p and change in temperature T can be written as follows[30]

$$Gu_{i,jj} + (G+\lambda)u_{j,ji} + \alpha_p p_{,i} + \alpha_T T_{,i} + F_i = 0, \tag{14}$$

and

$$\begin{cases} G = E/[2(1+\nu)] \\ \lambda = E\nu/[(1+\nu)(1-2\nu)] \\ p = S_w p_w + (1-S_w)p_c \\ F_i = \rho g \\ \rho = (1-n)\rho_s + nS_w\rho_w + n(1-S_w)\rho_c \end{cases} \tag{15}$$

where G is the shear modulus, u_i the displacement component in the ith direction ($i = x, y, z$), λ the lame constant, α_p (≤ 1) the corresponding Biot effective stress coefficient of the pore, $p_{,i}$ the pore pressure, α_T is the thermal expansion coefficient, $T_{,i}$ the change of the reservoir temperature, F_i the volume force in the ith direction, E the elastic modulus of the reservoir and ν is the Poisson ratio.

Dynamic evolution model of porosity and permeability

The porosity and permeability of a reservoir are key factors to describe fluid flow within the rock strata, which are closely related to the stress state and intrinsic properties of the rocks. The porosity and permeability of rock strata are influenced by ground stress, pore pressure and temperature. Considering the volume deformation caused by change in the framework particles and temperature, dynamic evolution models for porosity and absolute permeability respectively, can be represented as follows[31]

$$\varphi = 1 - \frac{(1-\varphi_0)(1-\Delta p/K_s + \alpha_T \Delta T)}{1+\varepsilon_v}, \tag{16}$$

$$k = \frac{k_0}{1+\varepsilon_v}\left[1 + \frac{\varepsilon_v - (1-\varphi_0)(\alpha_T \Delta T + \Delta p/K_s)}{\varphi_0}\right]^3, \tag{17}$$

where φ_0 is the initial porosity of the reservoir, $\varepsilon_v = \varepsilon_x + \varepsilon_y + \varepsilon_z$ the volume strain of the reservoir, Δp the increment of the pore pressure, ΔT the increment of temperature, K_s the volume modulus of the reservoir framework, and k_0 the initial absolute permeability of the strata.

Currently, the relative permeability models for porous media include the Van Genuchten Mulaem/Burdine (VGM&VGB) model, the Brooks and Corey Mulaem/Burdine (BCM&BCB) model, the lognormal distribution–Mualem (LNM) model, the Brutsaert–Burdine (BRB) model, and the Gardner–Mulaem model (GDM), among others. Among these, the VGM and BCB models are popular. The BCB model was selected to calculate relative permeability of water and CO_2 phase in this study, and the corresponding equations are given below[32,33]

$$k_{r,w} = k_{r,w0}\left(\frac{S_w - S_{r,w}}{1 - S_{r,w} - S_{r,c}}\right)^{3+\frac{2}{\lambda}}, \tag{18}$$

$$k_{r,c} = k_{r,c0}\left(1-\frac{S_w - S_{r,w}}{1-S_{r,w}-S_{r,c}}\right)^2\left[1-\left(\frac{S_w - S_{r,w}}{1-S_{r,w}-S_{r,c}}\right)^{1+\frac{2}{\lambda}}\right], \quad (19)$$

where $k_{r,w0}$ is the initial relative permeability of the water phase, $k_{r,c0}$ the initial relative permeability of the CO_2 phase, $S_{r,w}$ residual saturation of the water phase, $S_{r,c}$ residual saturation of the CO_2 phase and λ is a parameter representing the characteristics of pore structure in the reservoir.

Model verification

Computational procedure

Methods to calculate density, dynamic viscosity, specific heat capacity, heat conductivity coefficient, and dissolution of CO_2 under different temperatures and pressures are included in the proposed model. The deformation control equation of solid mechanics, the equation of motion of two-phase flow and the control equation of temperature fields based on energy conservation are also included in the model. The evaluation laws of porosity, absolute permeability, relative permeability and capillary force of rock strata at any given time are involved in the above three control equations. The pore pressure, strata deformation and fluid saturation at different times can be obtained by solving the THM coupled model using the finite element method (FEM). The fluid flow in rock strata will change the porosity, permeability and capillary force of the rocks. As a result, solution of the THM coupled model is nonlinear and an iterative method should be employed. COMSOL Multiphysics is a commercial software that can be used to numerically solve the PDE equation of the THM coupled model.

Verification of the fully coupled model

In CO_2 sequestration, migration velocity is measured by the horizontal distance between the intersection point of the CO_2–brine interface and the upper boundary of the aquifer to the well. The horizontal distance is referred to as the distance of the CO_2 migration front. The spatial distribution and distance of the CO_2 front in its sequestration were used to verify the THM model in this study. The parameters of the reservoir used to sequestrate CO_2 were as follows: length of the reservoir was 1000 m, thickness was 100 m, burial depth was 1500 m, and upper and bottom boundaries of the reservoir were impermeable. CO_2 was injected into the reservoir at a flow rate of 1 Mt/year. Figure 2 *a* shows the spatial distribution of CO_2 one year after injection[34]. Figure 2 *b* shows CO_2 distribution obtained by solving the THM coupled model under the same conditions. The distribution characteristics of CO_2 in Figure 2 *a* and *b* are the same. The distance of CO_2 migration front calculated by the THM coupled model was 618 m, which is close to the value (620 m) calculated by Vilarrasa *et al.*[34]. This difference between the two calculated distances of the CO_2 migration front is because continuous variation of density, dynamic viscosity, specific heat capacity, heat conductivity coefficient and solubility of CO_2 in water were considered in the THM coupled model. Figure 2 shows that the spatial distribution and migration velocity of CO_2 in the aquifer can be precisely predicted by the established THM coupled model. The figure also indicates that it is reliable and viable to study complex CO_2 injection by the THM coupled model.

Thermodynamic effect of supercritical CO_2 sequestration

Mathematical model and calculation parameters: The thickness of the saline aquifer was 100 m and burial depth was 1000 m. The hydrostatic pressure gradient within the aquifer was 0.01 MPa/m and the geothermal gradient was 0.01 K/m. The diameter of the CO_2 injection borehole was 0.1 m. As shown in Figure 3, the aquifer was located in the two-dimensional X–Z plane. The size of the aquifer was 1200 m × 100 m. The solved region

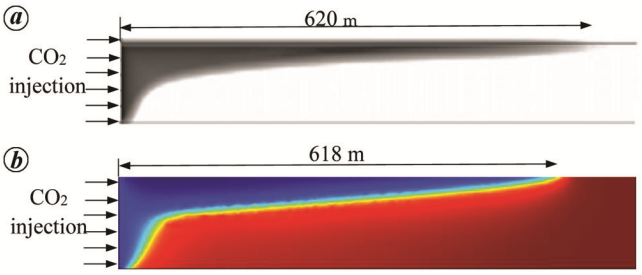

Figure 2. Spatial distribution and front distance of CO_2 migration within the reservoir after one year of CO_2 injection. ***a***, Results using the method of Vilarrasa *et al.*[34]. ***b***, Results using the thermo-hydro-mechanical (THM) coupling model.

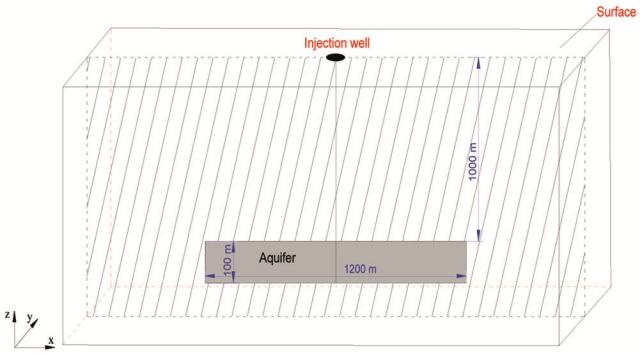

Figure 3. Schematic diagram of the 2D calculation region.

Table 1. Numerical simulation parameters

Parameter	Value	Source
Elastic modulus of the reservoir (E)	10 GPa	18
Reservoir Poisson's ratio (ν)	0.3	18
Reservoir density (ρ_s)	2200 kg/m^3	18
Reservoir specific heat capacity (C_s)	0.85 kJ/(kg K)	18
Reservoir heat conductivity coefficient (λ_s)	2.5 w/(m k)	11
Reservoir heat expansion coefficient (α_s)	1×10^{-5} 1/K	11
Initial porosity of the reservoir (φ_0)	0.2	18
Initial permeability of the reservoir (k_0)	1×10^{-16} m^2	18
Reservoir temperature (T)	273–373 K	18
Hydrostatic pressure (p_0)	5–25 MPa	18
Biot's coupled coefficient (α_p)	1	18
Characteristic parameter of reservoir pore construct (λ)	1	33
Density of water (ρ_w)	1000 kg/m^3	5
Dynamic viscosity of water (μ_w)	0.283 mPa s	5
Specific heat capacity (C_{pw})	4.2 kJ/(kg K)	5
Heat conductivity of water (λ_w)	0.67 w/(m k)	5
Residual saturation of water ($S_{r,w}$)	0.05	18
Compressibility factor of water (c_{wp})	1×10^{-9} 1/Pa	11
Heat expansion coefficient of water (c_{wpT})	4.5×10^{-5} 1/K	11
Density of CO_2 (ρ_c)	Calculated by continuous model in part 2.1	
Dynamic viscosity of CO_2 (μ_c)	Calculated by continuous model in part 2.2	
Specific heat capacity of CO_2 (C_{pc})	Calculated by continuous model in part 2.3	
Heat conductivity coefficient of CO_2 (λ_c)	Calculated by continuous model in part 2.4	
Solubility of CO_2 in water (ρ_{dc})	Calculated by continuous model in part 2.5	
Residual saturation of CO_2 ($S_{r,c}$)	0.05	18
Mass flow rate of CO_2 (q_c)	5 kg/s	18

was symmetrical about the injection borehole. To reduce the mesh element size and operational cost of the numerical simulation, a region with size 600 m × 100 m to the right of the injection well was selected as the solution region. Table 1 shows the related parameters of the numerical simulation.

Injection pressure of CO_2 under the THM coupled model

The injection pressure of CO_2 is the difference in pressure at the CO_2 injection point and the initial hydrostatic pressure or pore water pressure. The corresponding expression is[34]

$$p_{inj} = p_{c,inj} - p_{hyd,inj}, \tag{20}$$

where p_{inj} is the injection pressure of CO_2, $p_{c,inj}$ the pressure of CO_2 at the injection point and $p_{hyd,inj}$ is the initial hydrostatic pressure or pore water pressure.

Figure 4 shows the comparison results of CO_2 injection pressure calculated by the THM coupled model and the uncoupled model established by Sasaki *et al.*[18]. Figure 4 *a* shows that when the reservoir temperature is above 380 K, the CO_2 injection pressure calculated by the ideal gas EoS is close to the CO_2 injection pressure calculated by the Span and Wagner EoS. When the reservoir temperature is close to the critical temperature, the CO_2 injection pressure calculated by the ideal gas EoS is larger than that calculated by the Span and Wagner EoS.

As shown in Figure 4 *b* and *c*, the predicted CO_2 injection pressure by the THM coupled model is higher than that calculated by the uncoupled model. At a constant reservoir pressure and reservoir temperatures above 380 K, the difference between the two predicted CO_2 injection pressures decreases with increase in reservoir temperature. At a constant reservoir temperature, the difference of the two predicted values decreases with increase in reservoir pressure. Moreover, when the reservoir condition is close to the critical point of CO_2, the difference between the two predicted CO_2 injection pressures is relatively large because the phase change of CO_2 affects its injection pressure.

The preceding analysis shows that: (i) the injection pressure of CO_2 is highly sensitive to the reservoir temperature and pressure, and this is more obvious when the reservoir condition is close to the critical point of CO_2 and (ii) the injection pressure of CO_2 calculated by the uncoupled model, which is based on the ideal gas EoS, and Span and Wagner EoS is lower than that calculated by the THM coupled model. The calculation of the physical properties of CO_2, the phase of which continuously changes, has been taken into consideration in the THM coupled model. As a result, the calculation results of the THM coupled model should be more accurate than that of

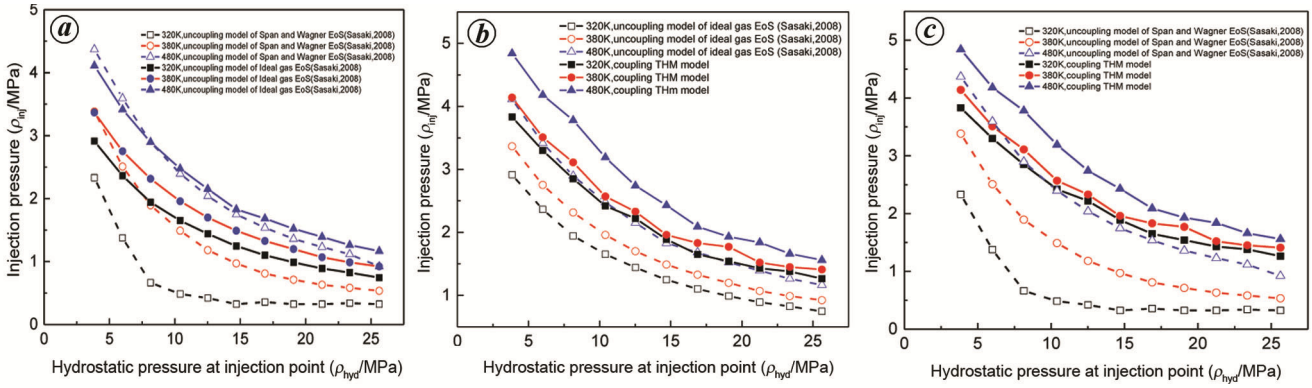

Figure 4. Relation between CO_2 injection pressure, and reservoir temperature and pressure. ***a***, Comparison of injection pressure calculated by the uncoupled model based on the ideal gas equation of state (EoS) and Span and Wagner EoS[34]. ***b***, Comparison of injection pressure calculated by the THM coupled model and uncoupled model based on the ideal gas EoS. ***c***, Comparison of injection pressure calculated by the THM coupled model and uncoupled model based on the Span and Wagner EoS.

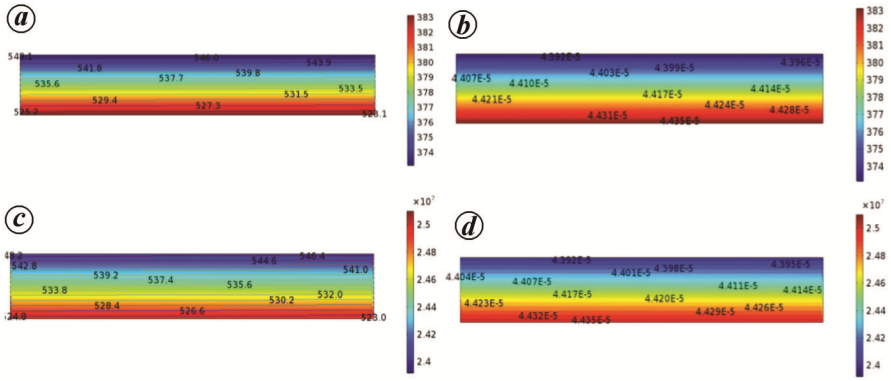

Figure 5. Density and dynamic viscosity of CO_2 under different temperatures and pressures. ***a***, Nephogram of reservoir temperature and density contour of CO_2. ***b***, Nephogram of reservoir temperature and dynamic viscosity contour of CO_2. ***c***, Nephogram of reservoir pressure and density contour of CO_2. ***d***, Nephogram of reservoir pressure and dynamic viscosity contour of CO_2.

the uncoupled model. It is necessary to verify the calculation error of the THM coupled model by field tests.

Spatial distribution of CO_2 in the THM coupled model

The temperature of injected CO_2 is usually lower than the reservoir temperature, and heat transfer between CO_2 and the reservoir will occur until the thermal transfer reaches an equilibrium state. Due to the existence of a geothermal gradient and hydrostatic pressure gradient within the reservoir, the density and dynamic viscosity of the injected CO_2 in the vertical direction is significantly different (Figure 5). After CO_2 injection, the density of CO_2 at the top boundary of the reservoir is larger than at the bottom boundary, whereas the dynamic viscosity of CO_2 at the upper reservoir is smaller than at the lower reservoir (Figure 5).

It can be seen from Figure 6 *a* that in the migration direction of CO_2, the saturation of CO_2 rapidly increases to a peak value and then slowly decreases. The saturation of CO_2 rapidly falls to the initial value, after which it is maintained at the same value. The saturation of CO_2 at the upper boundary of the reservoir was divided into four sections along the migration direction: the fast increase section, the slow decrease section, the fast decrease section and the initial saturation section. They are shown in Figure 7 as regions I, II, III and IV respectively. These four regions change with time.

The reasons for the existence of the fast increase section are as the follows: (i) CO_2 was still in a compressed state when it entered the reservoir. Since the reservoir temperature was higher than the temperature of CO_2, the compressed CO_2 would expand rapidly. (ii) The pressure of CO_2 at the bottom of the borehole was high, and compressed CO_2 was injected into the reservoir under high injection pressure. As a result, the amount of CO_2 in the reservoir around the bottom of the borehole rapidly increased in a short time. With continuous injection, the compressed supercritical CO_2 in the slow decrease region adapted to the reservoir environment. Finally, CO_2 migrated to the fast decrease region and the initial saturation region.

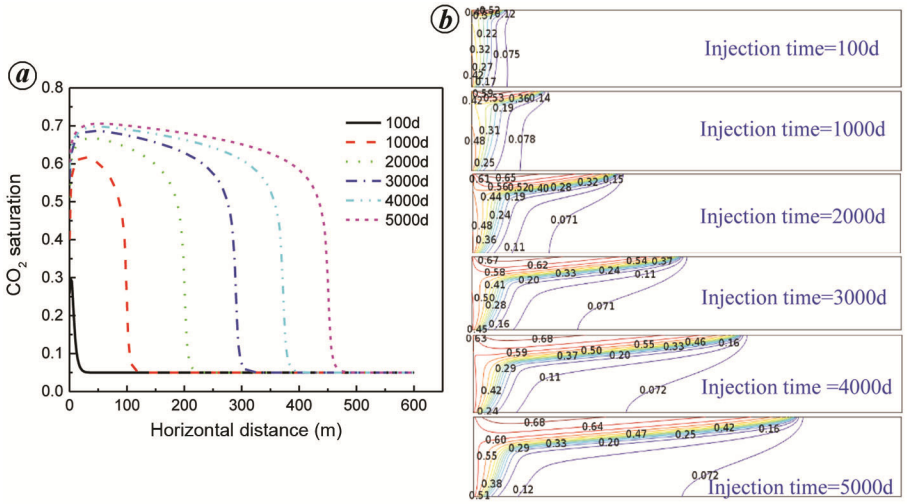

Figure 6. Variation of spatial distribution of CO_2 with time in the THM coupled model. ***a***, Distribution of CO_2 saturation along the top boundary of the reservoir. ***b***, Isoline distribution of CO_2 saturation at different times.

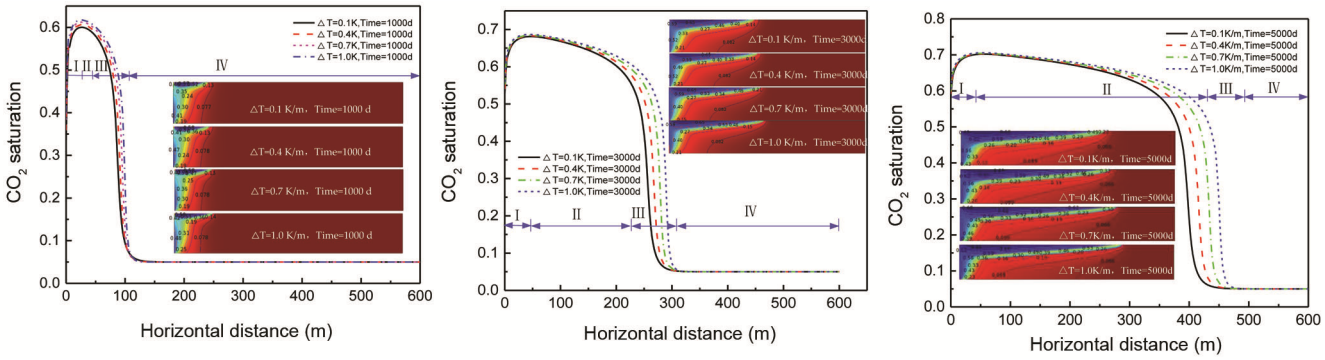

Figure 7. Distribution of CO_2 under different geothermal gradients.

Figure 6 *b* indicates that for any spatial point in the reservoir, the saturation of CO_2 at this point gradually increases with continuous migration into the reservoir. With regard to variation in the shape of the CO_2–brine interface with time, the longer the distance to the borehole, the larger is the front distance of CO_2 migration. Also, the CO_2–brine interface is correspondingly steeper because viscosity force in the lower part of the reservoir is larger than that in the upper part, and effect of viscosity force is stronger than that of gravity[33,35,36].

It can also be seen from Figure 7 that the fast decrease region is before the initial saturation region. This is because there is a mixed transition region between the injected well and the reservoir far from the well. The closer the mixed transition region to the well, less is the difference in the temperature and pressure. On the contrary, the farther the mixed transition region to the well, more is difference in the temperature and pressure between the injected CO_2 and the saline aquifer. Therefore, the fast decrease region comes before the initial saturation region.

Figure 7 also shows the spatial distribution of CO_2 saturation under geothermal gradients of 0.1, 0.4, 0.7 and 1.0 k/m. Analysis of saturability distribution curves of CO_2 at times of 1000, 3000 and 5000 d shows that a larger geothermal gradient corresponds to a greater distance of CO_2 migration front because with the increase in the geothermal gradient, the difference in dynamic viscosity of supercritical CO_2 in the upper and lower parts of the reservoir also increases. The dynamic viscosity of supercritical CO_2 in the upper reservoir is relatively small, and resistance of CO_2 flow in the upper reservoir is also small. Within the same time frame, the migration velocity as well as distance of the supercritical CO_2 migration front in the upper reservoir are larger. This phenomenon is termed the gravity override effect.

Figure 7 also indicates that at the same location, a larger geothermal gradient corresponds to a greater CO_2 saturation, because the reservoir temperature and pressure affect the density of CO_2 (Figures 1 *a* and 5 *a*, *c*). At constant pressure, the density of supercritical CO_2 is inversely

proportional to temperature. Since temperature in the upper reservoir is less than that in the lower reservoir, the density of supercritical CO_2 in the upper reservoir is larger than in the lower reservoir. The larger the geothermal gradient, greater is the temperature difference between the upper and lower reservoirs and the difference in CO_2 density is correspondingly larger. If the injection rate of CO_2 is constant, CO_2 density in the upper reservoir is larger than in the lower reservoir. As a result, more CO_2 could be stored in the upper reservoir compared to the lower reservoir. Within the same time-frame, the distance of CO_2 migration front in the upper reservoir is relatively larger.

In addition to reservoir temperature, the spatial distribution of CO_2 is also affected by the following factors: (i) CO_2 injected into the lower part of the brine aquifer with high temperature would flow upward along the CO_2–brine interface; (ii) brine in the upper aquifer with lower temperature would flow downwards along the CO_2–brine interface; (iii) the temperature of CO_2 will decrease because of the Joule–Thomson effect after CO_2 enters the reservoir from the borehole, and (iv) the dissolution of CO_2 in brine is a heat-release process. All these factors will slightly increase the temperature of supercritical CO_2 and affect the distribution[7].

Conclusion

The injection pressure of CO_2 is highly sensitive to reservoir temperature and pressure, and this sensitivity becomes more significant when the reservoir conditions are close to the critical point. Compared with CO_2 injection pressure calculated by the THM coupled model in this study, the injection pressure of CO_2 calculated by an uncoupled model based on the ideal gas EoS, and Span and Wagner EoS was relatively low. The THM coupled model was established based on the continuous calculation of physical property parameters of gaseous, liquid and supercritical CO_2. Therefore, the THM coupled model can be used to truly reflect the process of multiphase flow and heat flow, and to accurately predict the injection pressure.

Under the THM coupled function, the spatial distribution of CO_2 is characterized by the obvious gravity override along the vertical direction. Different CO_2 saturability regions occur along its migration direction at the top boundary of the saline aquifer, i.e. fast increase region, slow decrease region, fast decrease region and initial saturation region. The larger the geothermal gradient, greater is the CO_2 saturation at the top boundary of the reservoir; the reservoir space needed to sequester CO_2 is correspondingly smaller. The reason for CO_2 spatial distribution is that the physical property parameters such as density and dynamic viscosity of CO_2 are influenced by the reservoir temperature and pressure.

Conflicts of interest: The authors declare no conflict of interest.

1. Nwachukwu, A., Min, B. and Sriniyasan, S., Model selection for CO_2 sequestration using surface deformation and injection data. *Int. J. Greenhouse Gas Control*, 2017, **56**, 67–92.
2. Kim, S. and Hosseini, S. A., Study on the ratio of pore-pressure/stress changes during fluid injection and its implications for CO_2 geologic storage. *J. Pet. Sci. Eng*., 2017, **149**, 138–150.
3. Jiang, P., Li, X. and Xu, R., Thermal modeling of CO_2 in the injection well and reservoir at the Ordos CCS demonstration project, China. *Int. J. Greenhouse Gas Control*, 2014, **23**, 135–146.
4. Brassard, P., Godbout, S. and Raghavan, V., The production of engineered biochars in a vertical auger pyrolysis reactor for carbon sequestration. *Energies*, 2017, **10**, 288.
5. Yin, S., Dusseault, M. B. and Rothenburg, L., Coupled THMC modeling of CO_2 injection by finite element methods. *J. Pet. Sci. Eng*., 2011, **80**, 53–60.
6. Zhan, J. *et al.*, Decomposition analysis of the mechanism behind the spatial and temporal patterns of changes in carbon bio-sequestration in China. *Energies*, 2012, **5**, 386–398.
7. Li, C. and Laloui, L., Coupled multiphase thermo-hydro-mechanical analysis of supercritical CO_2 injection: benchmark for the in Salah surface uplift problem. *Int. J. Greenhouse Gas Control*, 2016, **51**, 394–408.
8. Hou, Z., Gou, Y. and Taron, J., Thermo-hydro-mechanical modeling of carbon dioxide injection for enhanced gas-recovery (CO_2–EGR): a benchmarking study for code comparison. *Environ. Earth Sci*., 2012, **67**, 549–561.
9. Li, J., Chen, A. and Yan, Y., Numerical simulation of carbon dioxide migration in a sandstone aquifer considering the fluid–solid coupling. *Acta Geotech*., 2014, **9**, 101–108.
10. Li, Q., Wu, Z. and Bai, Y., Thermo-hydro-mechanical modeling of CO_2 sequestration system around fault environment. *Pure Appl. Geophys*., 2006, **163**, 2585–2593.
11. Li, S., Li, X. and Zhang, D., A fully coupled thermo-hydro-mechanical, three-dimensional model for hydraulic stimulation treatments. *J. Nat. Gas Sci. Eng*., 2016, **34**, 64–84.
12. Fang, Y., Ba, N. N. and Carroll, K., Development of a coupled thermo-hydro-mechanical model in discontinuous media for carbon sequestration. *Int. J. Rock Mech. Min. Sci*., 2013, **62**, 138–147.
13. Basirat, F., Fagerlund, F. and Denchik, N., Numerical modelling of CO_2 injection at small-scale field experimental site in Maguelone, France. *Int. J. Greenhouse Gas Control*, 2016, **54**, 200–210.
14. Khan, S., Al-Shuhail, A. A. and Khulief, Y. A., Numerical modeling of the geomechanical behavior of Ghawar Arab-D carbonate petroleum reservoir undergoing CO_2 injection. *Environ. Earth Sci*., 2016, **75**, 1499.
15. Liu, H., Hou, Z. and Were, P., Numerical investigation of the formation, displacement and caprock integrity in the Ordos Basin (China) during CO_2 injection operation. *J. Pet. Sci. Eng*., 2016, **147**, 168–180.
16. Du, Z., Lin, W. and Gu, J., Numerical investigation for heat transfer of supercritical CO_2 cooled in a vertical circular tube. *Heat Transfer Eng*., 2012, **33**, 905–911.
17. Joshi, A., Gangadharan, S. and Leonenko, Y., Modeling of pressure evolution during multiple well injection of CO_2 in saline aquifers. *J. Nat. Gas Sci. Eng*., 2016, **36**, 1070–1079.
18. Sasaki, K., Fujii, T. and Niibori, Y., Numerical simulation of supercritical CO_2 injection into subsurface rock masses. *Energy Convers. Manage*., 2008, **49**, 54–61.
19. Aavatsmark, I., Kometa, B. K. and Gasda, S. E., A generalized cubic equation of state with application to pure CO_2 injection in aquifers. *Comput. Geosci.*, 2016, **20**, 623–635.

20. Youssef, Z., Barreau, A. and Mougin, P., Measurements of hydrate dissociation temperature of gas mixtures in the absence of any aqueous phase and prediction with the cubic–plus–association equation of state. *J. Chem. Eng. Data*, 2010, **55**, 2809–2814.
21. Peng, D. Y. and Robinson, D. B., A new two-constant equation of state. *Ind. Eng. Chem. Fundam.*, 1976, **15**, 92–94.
22. Wu, X., Wang, Q. and He, Y., Temperature–pressure field coupling calculation model considering phase behavior change in CO_2 injection well borehole. *J. China Univ. Pet. (Edn. Nat. Sci.),* 2009, **1**, 73–77.
23. Jossi, J. A., Stiel, L. I. and Thodos, G., The viscosity of pure substances in the dense gaseous and liquid phases. *Aiche J.*, 1962, **1**, 59–63.
24. Poling, B. E., Prausnitz, J. M. and O'Connell, J. P., *The Properties of Gases and Liquids*, McGraw-Hill, New York, USA, 2001, 5th edn, pp. 6.1–6.33.
25. Guo, X., Rong, S. and Yang, J., The viscosity model based on PR equation of state. *Acta Pet. Sin*., 1999, **3**, 64–69.
26. Shi, J., The distribution of temperature and pressure and injection string check of the injection and production wellbore of CO_2 flooding. China University of Petroleum-Beijing, Beijing, China, 2009, pp. 12–30.
27. Schnepper C. A. and Stadtherr, M. A., Robust process simulation using interval methods. *Comput. Chem. Eng*., 1996, **20**, 187–199.
28. Wang, L. and Liu, Y., Simulation on characteristics of supercritical fluid flow in porous media imposed temperature profiles. *Chem. React. Eng. Technol*., 1996, **20**, 187–199.
29. Zirrahi, M., Hassanzadeh, H. and Abedi, J., Prediction of CO_2 solubility in bitumen using the cubic-plus-association equation of state (CPA-EoS). *J. Supercrit. Fluids*, 2015, **98**, 44–49.
30. Chung, F. T., Jones, R. A. and Nguyen, H. T., Measurements and correlations of the physical properties of CO_2/heavy-crude-oil mixtures. *Spe. Reserv. Eng*., 1988, **3**, 822–828.
31. Kong, X., *High Seepage Mechanical*, Press of University of Science and Technology of China, Hefei, 2010, pp. 11–79.
32. Li, P., Kong, X. and Lu, D., Mathematical modeling of flow in saturated porous media on account of fluid-structure coupling effect. *J. Hydrodyn*., 2003, **4**, 419–426.
33. Chen, J., Hopmans, J. W. and Grismer, M. E., Parameter estimation of two-fluid capillary pressure–saturation and permeability functions. *Adv. Water Resour*., 1999, **22**, 479–493.
34. Vilarrasa, V., Silva, O. and Carrera, J., Liquid CO_2 injection for geological storage in deep saline aquifers. *Int. J. Greenhouse Gas Control*, 2013, **14**, 84–96.
35. Vilarrasa, V., Koyama, T. and Neretnieks, I., Shear-induced flow channels in a single rock fracture and their effect on solute transport. *Transp. Porous Media*, 2011, **87**, 503–523.
36. Lu, C., Lee, S. Y., and Han, W. S., Comments on 'abrupt-interface solution for carbon dioxide injection into porous media' by M. Dentz and D. Tartakovsky. *Transp. Porous Media*, 2009, **79***,* 29–37.

ACKNOWLEDGEMENTS. This work was supported by the Transformation of Scientific and Technological Achievements Programs (TSTAP) of Higher Education Institutions in Shanxi (No. 2020CG050), the Special Project of 2019 Plan for the Introduction of High-Level Scientific and Technological Talents in Development Zone of Lvliang City (development of automatic disassembly platform for hydraulic support pin shaft) (No. 2019L0002) and the Science and Technology Project of Lvliang City in 2019 (Pressure relief and permeability improvement technology by integrated hydraulic flushing and cutting for low permeability coal seam containing methane) (No. 2019L0008).

Received 30 May 2019; revised accepted 15 June 2020

doi: 10.18520/cs/v119/i6/973-983